THE JOURNAL OF PHYSICAL CHEMISTRY B

Article

pubs.acs.org/JPCB

Sorting Short Fragments of Single-Stranded DNA with an Evolving Electric Double Layer

Jiamin Wu,[†] Shuang-Liang Zhao,[‡] Lizeng Gao,[†] Jianzhong Wu,*[,§] and Di Gao*[,†]

[†]Department of Chemical and Petroleum Engineering, University of Pittsburgh, Pittsburgh, Pennsylvania 15261, United States

[‡]State Key Laboratory of Chemical Engineering, East China University of Science and Technology, Shanghai, 200238, China

[§]Department of Chemical and Environmental Engineering, University of California, Riverside, California 92521, United States

Supporting Information

ABSTRACT: We demonstrate a new procedure for separation of single-stranded DNA (ssDNA) fragments that are anchored to the surface of a gold electrode by end hybridization. The new separation procedure takes advantage of the strong yet evolving nonuniform electric field near the gold surface in contact with a buffer solution gradually being diluted with deionized water. Separation of short ssDNA fragments is demonstrated by monitoring the DNA at the gold surface with *in situ* fluorescence measurement. The experimental results can be rationalized with a simple theoretical model of electric double layer that relates the strength of the surface pulling force to the ionic concentration of the changing buffer solution.

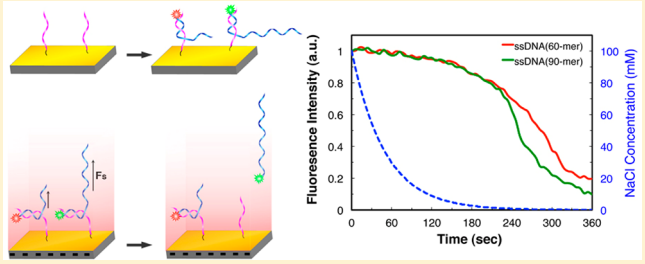

INTRODUCTION

Technological advances in micro/nanotechnology and high-resolution imaging systems empower the direct control of DNA molecules on surfaces by various means such as electric fields,[1,2] hydrodynamic flows,[3] magnetic[4,5] and optical tweezers,[6,7] micropipets,[8] and atomic force microscope (AFM) methods.[9,10] Due to the intrinsic negative charges present on the DNA backbone, the use of an electric field is particularly powerful, efficient, and convenient to manipulate surface-immobilized DNA molecules in an aqueous solution. Electrical control of DNA molecules offers many advantages since they can be readily implemented in a massively parallel way, thus suitable for high-throughput and multiplexing tasks. In particular, electrode-tethered DNA molecules can be efficiently manipulated at very low applied electrode potentials, taking advantage of the couterion-screened electric field that is significant within only a few Debye lengths from the surface. Despite the extremely strong electric field at the electrode/solution interface, the electric current is limited to a capacitive, non-Faradaic charging process. Such approaches have been successfully utilized for dynamic electrical switching of DNA layers[11] with applications in the highly sensitive label-free sensing of specific DNA sequences and proteins,[12,13] accelerating hybridization and selectively melting of mismatched DNA duplex,[14,15] and measurement of electrically induced conformational changes of end-tethered DNA molecules on electrode surfaces.[16−18]

Previously we have reported a novel DNA separation method by tethering DNA chains to a solid surface and then stretching the DNA chains with an electric field.[2,19,20] The anchor is such designed that the critical force to detach the DNA strand is independent of the chain length. Because the stretching force applied to the DNA strand is proportional to the net charge, a gradual increase of the electric field leads to a size-based separation of the DNA strands. Efficient separation of lambda DNA (48502 base pairs) from human genomic DNA (>100000 base pairs) has been demonstrated using this method.[19] Compared to current electrophoresis-based separation technologies, this method has the following advantages: it does not require separation matrices such as gels or polymer solutions, separated DNA can be readily recovered, and in principle, there is no upper limit on the length of DNA that can be separated. However, when this method is applied to separation of short single-stranded DNA (ssDNA), for example, with less than 100 nucleotides, a very strong electric field (on the order of 10^5 V/m) is needed to pull the DNA strands off the substrate. In practice, applying such a strong electric field may cause various technical problems such as Joule heating and side electrochemical reactions. Previously, we have used microfluidic narrow channels filled with a buffer of low ionic conductivity to apply such a strong electric field along the microfluidic channels (with negligible Joule heating) for separation of short ssDNA strands tethered to an insulating glass surface of the channels.[2] Here we demonstrate a new procedure for separation of short ssDNA fragments by taking the advantage of the strong yet evolving nonuniform electric field near the Au surface in contact with a buffer solution that is gradually diluted with deionized water.

We show that by tethering the ssDNA strands to an Au electrode and applying a relatively low electrode potential on

Received: September 28, 2012
Revised: January 17, 2013
Published: January 28, 2013

   dx.doi.org/10.1021/jp3096715 | J. Phys. Chem. B 2013, 117, 2267−2272

the Au electrode, ssDNA strands of different lengths can be separated by gradually diluting the buffer solution in contact with the Au electrode. The high electric field strength inside the electrical double layer at the gold/electrolyte interface allows us to pull short ssDNA strands off the surface with a very low electrode potential. Electrochemical reactions are avoided by maintaining the low electrode potential within the ideally polarizable region. Tuning the ion concentration of the electrolyte solution allows regulation of the nonuniform electric field. By gradually decreasing the ion concentration, longer ssDNA strands are detached first and then followed by the shorter ones. A numerical analysis based on a simple electric double layer model provides a semiquantitative explanation of the experimental results.

MATERIALS AND METHODS

Fabrication of Gold Electrodes. P-type silicon (100) wafers (0.001 Ω•cm, from Siltronix Corp.) were first coated with a 10 nm Ti adhesive layer, and then a 200 nm thick of gold film by using electron beam evaporation (VE-180, Thermionics Laboratory Inc., Hayward, CA). Pieces (10 mm × 10 mm) were cut from the gold coated wafer and used as electrodes. The electrodes were cleaned in a Piranha solution (mixture of H_2SO_4 and 30 w.t.% H_2O_2 at a weight ratio of 7:3, CAUTION: Piranha solution is a strong oxidant and must be handle with extreme caution) for 10 min, thoroughly rinsed with deionized water (Millipore, 18.2 MΩ), and dried with nitrogen before use.

Oligonucleotide Sequences. All oligonucleotides were purchased from Integrated DNA Technologies. The sequence of each 60-mer oligonucleotide was 5′-Alexa 647-*AATATTAAATTCATCTTC*TGTCCCTTCCCAGAAAACCTACCAGGGCAGCTACGGTTTCCG-3′; the 90-mer oligonucleotide sequence was 5′-Alexa 488-*AATATTAAATTCATCTTC*TGTCCCTTCCCAGAAAACCTACCAGGGCAGCTACGGTTTCCGTCTGGGCTTCTTGCATTCTGGGACAGCCAA-3′. Both oligonucleotides have no significant self-complementarity. The thiolated probe oligonucleotides (5′ HS-$(CH_2)_6$-TT*GAAGATGAATTTAATATT*-3′) were treated by adding 1 μM tris(2-chloroethyl) phosphate to disrupt formation of disulfide bonds between the thiol linkers.

Immobilization of DNA Probes on the Gold Electrode. Thiolated ssDNA probes (2 μM) were immobilized on the surface of freshly prepared gold electrodes in a high-salt buffer (1 M potassium phosphate buffer pH 7.0) through thiol-gold covalent bonding. Immobilization was completed after 24 h of incubation at room temperature. Afterward, the electrode was rinsed with deionized water. Mercaptohexanol (MCH) was then deposited onto the gold surface by exposing the electrode to an aqueous solution containing 1 mM MCH for ∼30 min. The formation of a MCH layer passivates the gold electrode and reduces nonspecific interactions between DNA and the gold surface during the subsequent hybridization step.[21] The surface density of the ssDNA probes immobilized on the gold surface was quantified according to a coulometric method reported by Steel, et al.[22] Briefly, chronocoulometry was performed in 10 mM tris buffer (pH 7.4) in the presence or absence of 50 μM $[Ru(NH_3)_6]^{3+}$ with a pulse period of 4 s and a pulse width of 500 mV (from 0.15 V to −0.45 V vs Ag/AgCl). A platinum wire was used as the reference electrode. The solutions were thoroughly purged with nitrogen prior to the experiments. In this method, $[Ru(NH_3)_6]^{3+}$ binds electrostatically to the phosphate groups on the DNA probe. Assuming that the charge on the phosphate groups is entirely compensated by $[Ru(NH_3)_6]^{3+}$, the surface density of DNA probes can be calculated from the charge of the DNA bound $[Ru(NH_3)_6]^{3+}$, which was obtained from the difference between the intercepts in chronocoulograms in the absence and presence of $[Ru(NH_3)_6]^{3+}$.

DNA Hybridization. Before hybridization, the gold electrodes with immobilized ssDNA probes were thoroughly washed with deionized water. The surface density of DNA probes on the surface is measured to be about 3×10^{12} molecules/cm^2 (see Supporting Information). Target ssDNA (2 μM, equal molar mixture of the 90-mer and 60-mer oligonucleotides) in hybridization buffer (1 M NaCl, 10 mM phosphate buffer, pH 7.5) was applied onto the electrode, which was then incubated at 25 °C for 24 h. During the hybridization step, the DNA fragments are less likely to form clusters on the surface not only because of the electrostatic repulsion and the lack of complementary but also because the average spacing between two neighboring DNA probes (∼7 nm) is much larger than the DNA cross-section diameter. Finally, hybridized chips were sequentially rinsed with 0.1% Tween-20 in 1 M NaCl, 10 mM phosphate buffer (pH 7.5), and the hybridization buffer (1 M NaCl, 10 mM phosphate buffer, pH 7.5).

Fabrication of Electrochemical Flow Cell and In situ Fluorescence Monitoring. Figure 1a schematically shows the custom-built electrochemical flow cell designed for stretching immobilized DNA at the gold electrode surface and for *in situ* fluorescence imaging of the gold electrode surface under an electric field. The cell consists of a cylindrical chamber 5 mm in diameter and 2.5 mm in depth, and is centered on a 2.5 mm thick poly(methyl methacrylate) (PMMA) plate. An inlet and an outlet for the fluid were drilled from the side edges of the PMMA plate to the chamber wall, to allow fluid flow through the chamber. The DNA-modified gold surface was used as the working electrode and sealed with an O-ring on the bottom of the chamber. An ITO-coated glass, which serves as the counter electrode, was pressed on top of the chamber to complete the flow cell. The cell was first filled with detection buffer of a high ionic strength (100 mM NaCl aqueous solution) using a syringe pump. After 10 min incubation in the dark, a negative voltage (−300 mV) was applied to the working electrode. The deionized water was continuously introduced into the flow cell at a rate of 60 μL/min while the temperature was kept at 15 °C.

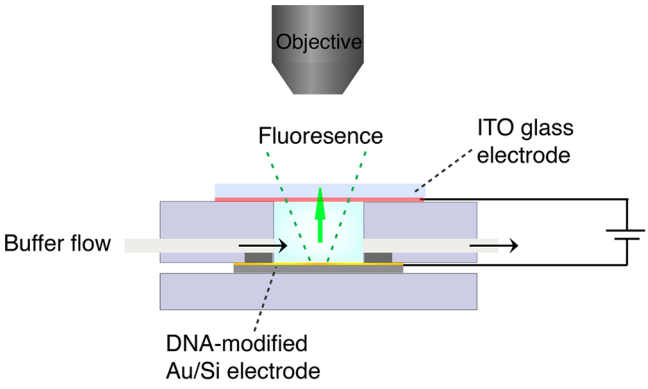

Figure 1. Schematic of the custom-built electrochemical flow cell designed for stretching DNA immobilized on the gold electrode and in situ fluorescence imaging of the gold electrode surface under an electric field.

dx.doi.org/10.1021/jp3096715 | J. Phys. Chem. B 2013, 117, 2267−2272

Departing of ssDNA from the surface was monitored in real-time by a fluorescence microscope. Fluorescence images were taken and analyzed using image analysis software.

RESULTS AND DISCUSSION

Figure 2 shows schematically the experimental procedure employed in this work for separation of DNA fragments by

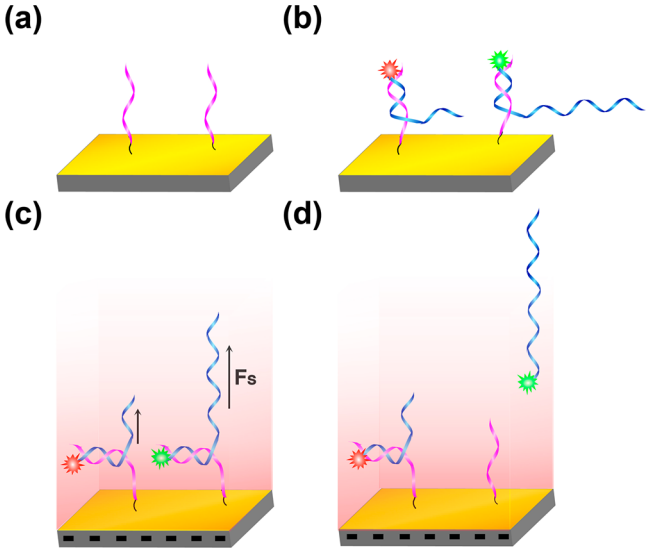

Figure 2. Schematic procedure for sorting ssDNA fragments by stretching in an electric field near a charged gold surface. (a) ssDNA probes are immobilized to the gold electrode surface. (b) Fluorophore-labeled target ssDNA strands of different lengths, with a common tail complementary to the ssDNA probes, hybridize with the ssDNA probes on the gold surface. (c) Electrically induced ssDNAs unzipping from the probe immobilized on the charged gold electrode. (d) ssDNA strands are separated by length.

stretching in a nonuniform electric field near a charged gold surface. ssDNA probes were first immobilized to the gold surface (Figure 2a) at a number density of $\sim 3 \times 10^{12}$ /cm^2 (see Figure S1 in Supporting Information). Then, fluorophore-labeled target ssDNA strands of different lengths, with a common tail of 18 bases long at the 5′ end complementary to the ssDNA probe, were allowed to hybridize with the ssDNA probe on the gold surface (Figure 2b). Afterward, the gold electrode was mounted in a custom-built electrochemical flow cell (shown in Figure 1). A DC voltage (300 mV) was applied between the counter electrode and the gold electrode. The fluorescence intensity of the gold electrode surface was monitored in real time while reducing the ionic strength of the detection buffer solution by introducing deionized water into the channel at a flow rate of 60 μL/min. At this flow rate, the hydrodynamic force, compared to the electrostatic force, applied to the DNA strands can be neglected. With a potential drop of 300 mV across the cell, the current was limited to non-Faradic processes, and thus detrimental electrochemical reactions may be avoided.

Figure 3a shows the fluorescence responses of 60-mer ssDNA and 90-mer ssDNA to a gradual reduction of the ionic strength of detection buffer with 300 mV potential drop across the cell. At high ionic strength (i.e., when the NaCl concentration in the buffer drops from 100 mM down to several mM), the fluorescence intensities of ssDNA strands of both lengths gradually decrease as the ionic strength falls, but

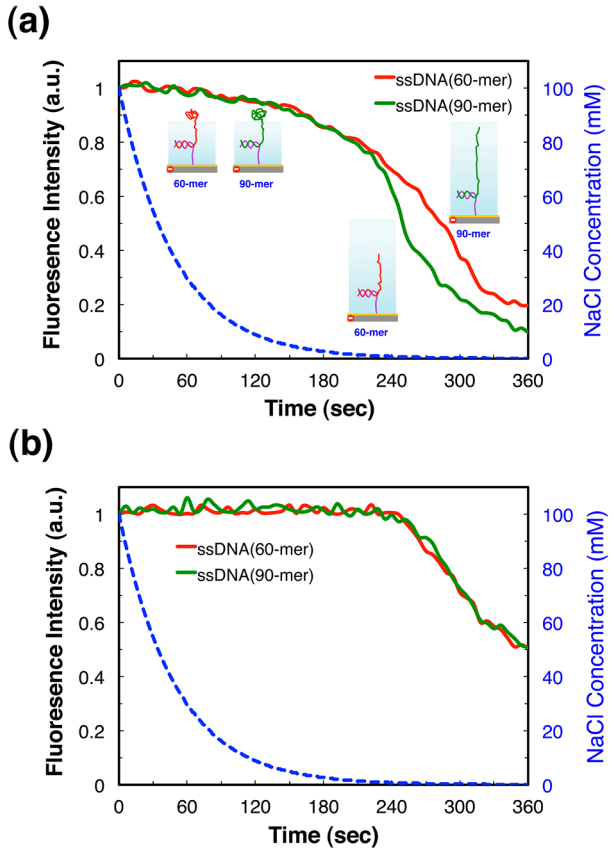

Figure 3. Fluorescence responses of 60-mer and 90-mer ssDNAs tethered to the gold surface as a function of buffer concentration. (a) A 300 mV potential drop is applied across the cell. (b) Control experiment (no potential drop is applied).

no significant difference is observed between the two plots. When the NaCl concentration drops to around 1.05 mM, the fluorescence intensity of the longer ssDNA (90-mer) starts to decay faster than that of the shorter one (60-mer). In this case, the fluorescence response profiles of the two ssDNA strands are obviously separated.

Figure 3b shows the result of a control experiment, where the fluorescence responses of the ssDNA strands to a gradual reduction in the ionic strength of detection buffer are monitored without applying a potential drop across the cell. In this condition, it is found that the fluorescence response is independent of the ssDNA strand length. The normalized fluorescence intensity profiles of the two ssDNA strands are almost identical. The fluorescence signal remains constant as the ionic strength gradually decreases to 0.60 mM, after which the fluorescence intensity drops significantly for both ssDNA strands. The sudden drop of fluorescence intensity indicates that ssDNA strands of both lengths begin to dissociate from the probe and depart from the surface. The dissociation at the anchoring position is likely because that, as the ionic strength decreases, the charges along DNA backbone become less shielded by counterions, making the dsDNA duplex less stable.[23,24] Compared with the control experiment, it is clear that stretching DNA near a charged surface can separate ssDNA strands according to the size.

The different fluorescence responses observed when stretching the ssDNA strands of two different lengths may be explained by a simple electric double layer model. In the presence of an electric potential, the Au electrode is in contact

dx.doi.org/10.1021/jp3096715 | J. Phys. Chem. B 2013, 117, 2267−2272

with an electric double layer (EDL) with a sharp gradient of the electric field. The inhomogeneous electric field exerts a pulling force on the DNA chains due to the presence of the backbone charge.[25,26] Apparently the magnitude of pulling force is not only related to the number of nucleotides (N) but also to the nonlocal electric field. Since the electric field varies with the ion concentration, which is time-dependent due to the introduction of deionized water, the pulling force, here designated as $F[N,t]$, depends on both time and the DNA chain length. Clearly, an explicit expression for $F[N,t]$ will provide insights into the separation mechanism and thus an explanation of the experimental results.

To seek a simple expression for $F[N,t]$, we assume that the tethered DNA chains are uncorrelated. Although a more accurate description can be obtained by, for example, using the density functional theory,[27,28] this assumption greatly simplify the problem at hand while it can still, as we shall see, provide meaningful insight into the experiment results. Under this assumption, the distribution of electric potential can be obtained by following the conventional knowledge of the electric double layer. Whereas it has been shown that the density functional theory provides a robust tool to investigate the electric double layer at various ion concentrations,[29,30] we conjecture that for the problem at hand the Poisson–Boltzmann (PB) equation should be sufficient because both the surface density of tethered DNA fragments ($\sim 3 \times 10^{12}$ /cm^2) and the ion concentration (less than 100 mM) are very small.[29]

In a coordinate system with the Au surface as the xy plane and the normal direction pointing to the solution as the z axis (see the inset of Figure 4), the electric potential changes only along the z direction. For a NaCl solution in contact with a planar electrode, the PB equation is given by

$$\frac{d^2\phi(z)}{dz^2} = \frac{2e\rho^0}{\varepsilon}\sinh\left[\frac{e\phi(z)}{k_BT}\right] \tag{1}$$

where ρ^0 is the salt concentration in the bulk, k_B is Boltzmann constant, T is the temperature solution, and $\varepsilon = \varepsilon_r\varepsilon_0$ is the dielectric constant. In this work, we take $\varepsilon_r = 82.0$ for saline water.[31] Although the presence of MCH self-assembled monolayer (SAM) on gold surface will generate a significant potential drop across the SAM, recent study[32] showed that in the column volume perpendicular to gold surface around defect sites (i.e., the places where thiolated ssDNA probes are bonded), the electric potential distribution remains nearly the same as that without the presence of SAM. In other words, in the interested volume along z direction starting from defect sites, the potential drop across SAM is irrelevant. Since the distance between two electrodes (Au surface and counter electrode) is on macroscopic level, it is reasonable to use the following boundary conditions:

$$\left.\frac{d\phi(z)}{dz}\right|_{z\to\infty} = 0;\ \phi(z)|_{z\to 0} = \phi^w \tag{2}$$

where ϕ^w denotes the surface potential. In dimensionless form, the PB equation can be written as

$$\frac{d^2y}{dz^2} = \kappa^2\sinh(y) \tag{3}$$

where $y = e\phi(z)/k_BT$, and $\kappa = (2\rho^0e^2/\varepsilon k_BT)^{1/2}$ is the Debye screening parameter. Equation 3 can be solved analytically[33]

$$y(z) = 2\ln\frac{1+\gamma e^{-\kappa z}}{1-\gamma e^{-\kappa z}} \tag{4}$$

with $\gamma = \tanh\left[e\phi^w/(4k_BT)\right]$.

In our experiment, the ion concentration ρ^0 in the bulk varies with time. If we denote the solution volume confined within the chamber as V, and the average volume flow rate as v, the mass conservation equation within the cell is given by:

$$\rho^0(t+\delta t)V = \rho^0(t)V - \rho^0(t)v\delta t \tag{5}$$

In writing the above equation, we assume that ion transport due to diffusion is negligible. In a differential form, eq 5 becomes

$$\frac{d\rho^0(t)}{dt} = -\frac{v}{V}\rho^0(t) \tag{6}$$

An integration of eq 6 gives

$$\rho^0(t) = 99.65\exp(-0.0236t) + 0.35 \tag{7}$$

In deriving the above result, we have fitted parameters v and V from the experimental data $\rho^0(0) = 100$ mM, $\rho^0(210) = 1.05$ mM, and $\rho^0(254) = 0.6$ mM. The ion concentration versus time is plotted in Figure 3.

To find the stretching force due to a varying electric field, we assume that each ssDNA chain is fully extended to the solution before detaching from the Au surface. In other words, we treat each ssDNA chain as a linear "cord" perpendicular to surface with a charge density $\sigma = q_e/\lambda$. Here q_e is the effective charge on each nucleotide, and λ is the average extension between two nucleotides (or interbase distance in ssDNA). The total force pulling each chain can be calculated from

$$\begin{aligned} F[N,t] &= \sum_{i=1}^{N} q_eE[z_i,t] = -\sum_{i=1}^{N} q_e\frac{d\phi}{dz} = -\sum \sigma dz\frac{d\phi}{dz} \\ &= -\int_{z=L_0}^{z=L_0+N\lambda} \sigma d\phi(z,t) \\ &= \sigma[\phi(L_0,t) - \phi(L_0+N\lambda,t)] \end{aligned} \tag{8}$$

In eq 8, L_0 is the distance of the hybridized head of a stretched ssDNA chain to the surface, and its value is associated with the probe DNA. In this work, we take L_0= 1 nm, corresponding to the size of 5′ HS-$(CH_2)_6$- which does not

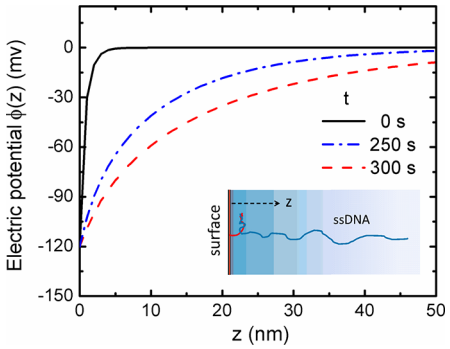

Figure 4. Calculated electric potential distribution along surface normal direction at three representative time point t = 0, 250, and 300 s based on a model electric double layer system. The inset sketches the model system.

dx.doi.org/10.1021/jp3096715 | J. Phys. Chem. B 2013, 117, 2267–2272

take part in the hybridization. From the first line to second line in eq 8, we changed the discrete summation into a continuous function. Although a ssDNA chain is flexible, the contour length and the interbase distance are insensitive to the solution conditions.[34,35] Here we adopt $\lambda = 0.42$ nm[34] since the ssDNA sequence is partially hybridized with the probe DNA. The effective charge of each nucleotide may vary slightly in different conditions[26] and for saline water we take $q_e = -0.25e$.[25]

Finally the surface potential ϕ^w is defined as the potential incensement from bulk to surface,[36] and its value is related to the excess charge density in Au/Si plate,[37] and in this work the surface potential is obtained by fitting the experimental results. To that end, we introduce a fluctuation force that results from the solvent effect, marked as F_f. As documented before,[2,20] F_f on tethered ssDNA takes Gaussian-like distribution and its mean value depends both on tethering detail and slightly on chain length. The detachment of ssDNA from surface is conditioned as

$$F_t = F + F_f \tag{9}$$

Here F_t is the tethering force, and in the current work it refers to the force required to break the target ssDAN from the probe, or equivalently the dsDNA unzipping force. On the other hand, the normalized intensity α, which scales the amount of ssDNAs remaining on the surface, is directly connected to fluctuation force distribution,

$$\alpha(t) = \int_{-\infty}^{F_t - F} \rho(F_f)\mathrm{d}F_f \tag{10}$$

which indicates that, during the process of gradual detachment, we should have

$$-\frac{d\alpha(t)}{dt} = \rho(F_t - F)\frac{dF}{dt} \tag{11}$$

Above equation gives the distribution of the fluctuation force, and with which one can calculate its mean value on 60-mer ssDNA and 90-mer ssDNA. Since the mean value is less sensitive to the chain length when it is large, we assume the mean value of fluctuation forces on 60-mer ssDNA and on 90-mer ssDNA are the same, and this leads to an equation determining the surface potential

$$\int_0^{400} (F_t - F[90, t])\frac{\mathrm{d}\alpha(t)}{\mathrm{d}t}\bigg|_{N=90} \mathrm{d}t = \int_0^{400} (F_t - F[60, t])\frac{\mathrm{d}\alpha(t)}{\mathrm{d}t}\bigg|_{N=60} \mathrm{d}t \tag{12}$$

With $F_t = 14$ pN, we get the best fit for surface potential $\phi^w = -120$ mV. Since the hydrated ion size is about 0.7 nm for sodium,[38] it is easy to check the saturation limit value for surface potential is about −160 mV. Whereas the standard Poisson−Boltzmann theory ignores the steric effect, the fact that fitted surface potential below the saturation limit value somewhat indicates the validity of its application.

The estimation of surface potential combining eq 4 and eq 7 gives the time-dependent electric potential distribution $\phi(z,t)$, which is presented in Figure 4 at three representative times (t = 0, 250, 300 s). While the contact value of electric potential is fixed, its gradient near the electrode surface varies sharply as the ion concentration decreases. In Figure 5, we plot the time-dependent pulling force on 90-mer ssDNA and 60-mer ssDNA. As time elapses, the pulling force on both 90-mer ssDNA (the red curve) and 60-mer ssDNA (the black curve) increases, and they remain identical until around 180 s. After that, the pulling force on 90-mer ssDNA rises more quickly than that on 60-mer ssDNA before both reach their own maximum. The difference in pulling forces explains why 90-mer ssDNA escapes from surface prior to 60-mer ssDNA.

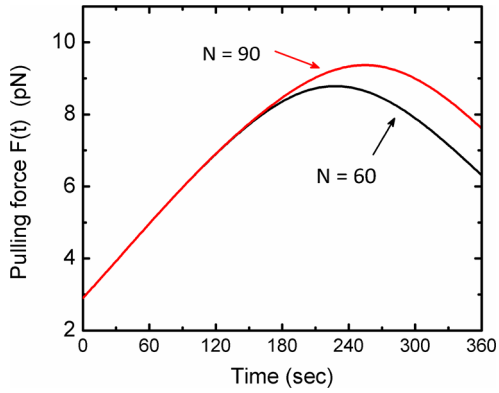

Figure 5. Calculated pulling forces on 60-mer and 90-mer ssDNAs versus time.

The results shown in Figures 4 and 5, as well as the pulling force expression in eq 8, may help us explain the separation mechanism. Because the charge density on ssDNA is fixed, eq 8 indicates that the magnitude of the pulling force depends only on the electric potential across the span of a single ssDNA chain. To facilitate the discussion, we mark the end near surface as A, and the other one as B. The corresponding electric potentials are $\phi(z_A)$ and $\phi(z_B)$, abbreviated as ϕ_A and ϕ_B, respectively. Obviously, for different ssDNA chain, ϕ_A is independent of the chain length due to the identical probe design. At the beginning of experiment, the ion concentration is relatively high, and the effective length of the electric double layer to solution is much smaller than the extended lengths of both 90-mer and 60-mer ssDNA. In that case, ϕ_B is approximately equal to zero for both ssDNAs, and ϕ_A is finite but identical for both chains. Thus the pulling forces that proportional to $(\phi_B - \phi_A)$ are the same. As the ion concentration decreases, the thickness of electric double layer increases. If it is still less than the extended lengths of both ssDNAs, we hold $\phi_B = 0$, and $(\phi_B - \phi_A)$ still the same for different chains. As shown in Figure 4, the gradient of the electric potential become smaller, and ϕ_A becomes more negative. That means in this period the strength of pulling force increases but still identical for both ssDNAs. When the effective length of electric field continues to increase, the head B of short ssDNA is covered by the electric potential, and ϕ_B has finite negative value for short ssDNA while still zero for long ssDNA. In this period, the potential drops for different lengths $(\phi_B - \phi_A)$ gradually become different, and the longer ssDNA undergoes a larger pulling force. If this pulling force is beyond the tethering force, the long ssDNA detaches from the electrode surface. Finally, if the ion concentration becomes sufficiently low, the head B of long ssDNA is also covered by the electric potential. In that case, ϕ_B has finite and negative value for both short and long ssDNAs. Because the value for short ssDNA is more negative, $(\phi_B - \phi_A)$ is smaller. In other words, the pulling force for long ssDNA is still larger than that for short ssDNA. In the limit case of infinite dilute ion concentration, the electric field $E = \phi^w/d$ where d is the distance of two parallel layers. In that case, the pulling force for ssDNA

dx.doi.org/10.1021/jp3096715 | J. Phys. Chem. B 2013, 117, 2267−2272

simply becomes $q_e\phi^w N/d$, and the system recovers to our previous experimental design.[2]

CONCLUSIONS

To conclude, we have developed a novel experimental procedure to separate ssDNAs according to the chain length. We demonstrated that by tethering ssDNA to a gold electrode and applying a relatively low electrode potential to the Au electrode and then gradually decreasing the ion concentration near the electrode, we can detach the tethered short ssDNA chains sequentially. The pulling force is different for ssDNA chains with different chain lengths, and thus with a careful design of the surface potential and the tethering detail, we are able to detach the longer ssDNA chains first and then the shorter ones. We have developed a simple analytical model to understand the experimental mechanism. With reasonable model parameters, the simple electric double layer model provides a semiquantitative explanation of the experimental results.

ASSOCIATED CONTENT

Supporting Information

We provide additional experimental details and data about the quantitative measurement of surface density of DNA probes. This material is available free of charge via the Internet at http://pubs.acs.org.

AUTHOR INFORMATION

Corresponding Author

*E-mail: jwu@engr.ucr.edu; gaod@pitt.edu.

Notes

The authors declare no competing financial interest.

ACKNOWLEDGMENTS

The authors acknowledge financial support from the National Institute of Health (R21-AI077532) and the National Science Foundation (CBET0747164).

REFERENCES

(1) Sosnowski, R. G.; Tu, E.; Butler, W. F.; O'Connell, J. P.; Heller, M. J. *Proc. Natl. Acad. Sci.* **1997**, *94*, 1119.
(2) Wu, J.; Zhao, S.-L.; Gao, L.; Wu, J.; Gao, D. *Lab Chip* **2011**, *11*, 4036.
(3) Perkins, T. T.; Smith, D. E.; Larson, R. G.; Chu, S. *Science* **1995**, *268*, 83.
(4) Smith, S.; Finzi, L.; Bustamante, C. *Science* **1992**, *258*, 1122.
(5) Gosse, C.; Croquette, V. *Biophys. J.* **2002**, *82*, 3314.
(6) Wang, M. D.; Yin, H.; Landick, R.; Gelles, J.; Block, S. M. *Biophys. J.* **1997**, *72*, 1335.
(7) Bustamante, C.; Bryant, Z.; Smith, S. B. *Nature* **2003**, *421*, 423.
(8) Cluzel, P.; Lebrun, A.; Heller, C.; Lavery, R.; Viovy, J.-L.; Chatenay, D.; Caron, F. *Science* **1996**, *271*, 792.
(9) Rief, M.; Clausen-Schaumann, H.; Gaub, H. E. *Nat. Struct. Mol. Biol.* **1999**, *6*, 346.
(10) Erdmann, M.; David, R.; Fornof, A.; Gaub, H. E. *Nat. Nano* **2010**, *5*, 154.
(11) Rant, U.; Arinaga, K.; Fujita, S.; Yokoyama, N.; Abstreiter, G.; Tornow, M. *Nano Lett.* **2004**, *4*, 2441.
(12) Rant, U.; Arinaga, K.; Scherer, S.; Pringsheim, E.; Fujita, S.; Yokoyama, N.; Tornow, M.; Abstreiter, G. *Proc. Natl. Acad. Sci.* **2007**, *104*, 17364.
(13) Rant, U.; Pringsheim, E.; Kaiser, W.; Arinaga, K.; Knezevic, J.; Tornow, M.; Fujita, S.; Yokoyama, N.; Abstreiter, G. *Nano Lett.* **2009**, *9*, 1290.
(14) Heaton, R. J.; Peterson, A. W.; Georgiadis, R. M. *Proc. Natl. Acad. Sci.* **2001**, *98*, 3701.
(15) Wong, I. Y.; Melosh, N. A. *Nano Lett.* **2009**, *9*, 3521.
(16) Murphy, J. N.; Cheng, A. K. H.; Yu, H.-Z.; Bizzotto, D. *J. Am. Chem. Soc.* **2009**, *131*, 4042.
(17) Kaiser, W.; Rant, U. *J. Am. Chem. Soc.* **2010**, *132*, 7935.
(18) Spuhler, P. S.; Knežević, J.; Yalçin, A.; Bao, Q.; Pringsheim, E.; Dröge, P.; Rant, U.; Ünlü, M. S. *Proc. Natl. Acad. Sci.* **2010**, *107*, 1397.
(19) Gao, L.; Wu, J.; Gao, D.; Wu, J. *Appl. Phys. Lett.* **2007**, *91*, 113902.
(20) Zhao, S.-L.; Wu, J.; Gao, D.; Wu, J. *J. Chem. Phys.* **2011**, *134*, 065103.
(21) Herne, T. M.; Tarlov, M. J. *J. Am. Chem. Soc.* **1997**, *119*, 8916.
(22) Steel, A. B.; Herne, T. M.; Tarlov, M. J. *Anal. Chem.* **1998**, *70*, 4670.
(23) Schildkraut, C.; Lifson, S. *Biopolymers* **1965**, *3*, 195.
(24) Tan, Z.-J.; Chen, S.-J. *Biophys. J.* **2006**, *90*, 1175.
(25) Keyser, U. F.; Koeleman, B. N.; Van Dorp, S.; Krapf, D.; Smeets, R. M. M.; Lemay, S. G.; Dekker, N. H.; Dekker, C. *Nat. Phys.* **2006**, *2*, 473.
(26) Zhang, J.; Shklovskii, B. I. *Phys. Rev. E* **2007**, *75*, 021906.
(27) Jiang, T.; Wu, J. Z. *J. Phys. Chem. B* **2008**, *112*, 7713.
(28) Jiang, T.; Li, Z. D.; Wu, J. Z. *Macromolecules* **2007**, *40*, 334.
(29) Lee, J. W.; Nilson, R. H.; Templeton, J. A.; Griffiths, S. K.; Kung, A.; Wong, B. M. *J. Chem. Theory Comput.* **2012**, *8*, 2012.
(30) Henderson, D.; Lamperski, S.; Jin, Z.; Wu, J. *J. Phys. Chem. B* **2011**, *115*, 12911.
(31) Strogryn, A. *IEEE Trans. Microwave Theory Tech.* **1971**, *MTT-19*, 733.
(32) Josephs, E. A.; Ye, T. *J. Am. Chem. Soc.* **2012**, *134*, 10021.
(33) Zimm, B. H.; Lebret, M. *J. Biomol. Struct. Dyn.* **1983**, *1*, 461.
(34) Ding, F.; Manosas, M.; Spiering, M. M.; Benkovic, S. J.; Bensimon, D.; Allemand, J.-F.; Croquette, V. *Nat. Methods* **2012**, *9*, 367.
(35) Ambia-Garrido, J.; Vainrub, A.; Pettitt, B. M. *Comput. Phys. Commun.* **2010**, *181*, 2001.
(36) Russel, W. B.; Saville, D. A.; Schowalter, W. R. *Colloidal Dispersions*; Cambridge University Press: Cambridge, 1992.
(37) Bard, A. J.; Faulkner, L. R. *Electrochemical Methods: Fundamentals and Applicaitons*, Second ed.; John Wiley & Sons Inc.: New York, 2001.
(38) Fellman, B. F. *Carbon-based electric double layer capacitor for water desalination*, S.M. Thesis; Massachusetts Institute of Technology: Cambridge, MA, 2010.